Efficient Generation of 3-D Capacitance Macromodel Based on Finite Difference Method

Ming Yang, Wenjian Yu
TNList, Dept. Computer Science and Tech., Tsinghua University, Beijing 100084, China
Email: ming-yang13@mails.tsinghua.edu.cn, yu-wj@tsinghua.edu.cn

***Abstract*—Capacitance macromodel is a novel idea recently proposed for encrypting sensitive structures and bringing acceleration in the capacitance extraction of integrated circuits. The existing technique of macromodeling employs boundary element method (BEM), but may lead to unreliable results due to computational error. In this work, we present the technique of generating the capacitance macromodel based on finite difference method (FDM). Numerical experiments with three-dimensional (3-D) structures show the FDM based technique is more reliable and efficient than BEM. And, the obtained capacitance matrix well satisfies the requirement for using the macromodel-aware floating random walk method in capacitance extraction.**

Keywords—capacitance extraction; capacitance macromodel; finite difference method; floating random walk; integrated circuit

I. INTRODUCTION

With the microfabrication process technology of integrated circuits (ICs) advancing, accurate 3-D field solver solution for the capacitance extraction of nanometer IC structures becomes more and more important. Among various techniques for field-solver capacitance extraction, the floating random walk (FRW) method has become popular due to its advantages in scalability, reliability, and parallelism [1-4]. Another challenge in capacitance extraction is the need of encrypting the structure information from foundry or IP vendor [5]. A recent work [3] solved this issue with a novel macromodel-aware FRW algorithm, which also accelerates the capacitance extraction for structure with cyclic layout patterns. Its basic idea is building a macromodel for each specified sensitive or cyclic sub-structure, and then connecting the Markov-chain random walk (MCRW) inside the macromodel and the FRW outside through a pre-characterized patch region.

The macromodel is essentially a closed-domain capacitance matrix, reflecting the electrostatic couplings among boundary panels of the inherent sub-structure. Suppose the boundary is partitioned into panels, and $\boldsymbol{U}$ and $\boldsymbol{Q}$ denote the vectors of electric potential and electric charge on boundary panels and inside conductors (if there are), respectively. The macromodel capacitance matrix $\boldsymbol{C}$ is symmetric, and satisfies:

$$\boldsymbol{Q} = \boldsymbol{C}\boldsymbol{U} . \quad (1)$$

Electrostatic theory infers that $\boldsymbol{C}$ has positive diagonal and negative off-diagonal entries, and the sum of each row/column equals to zero. This ensures that the ratios of capacitance entries can be regarded as probabilities so that the MCRW can be performed. However, the numerical method for calculating $\boldsymbol{C}$ may not ensure these properties due to computational error. For example, BEM employed in [3] often violates them. Although extra regularization may be applied, it induces new source of error and sometimes lead to large error in the result of macromodel-aware capacitance extraction.

In this work, we develop a 3-D FDM based technique for generating the macromodel. It handles actual IC structures and is more reliable for ensuring the properties of macromodel matrix. Efficient matrix computation techniques are also applied, resulting in shorter runtime than the BEM counterpart.

This work is supported by NSFC under grant No. 61422402.

II. FINITE DIFFERENCE METHOD FOR GENERATING 3-D CAPACITANCE MACROMODEL

A. Basic Formulas and Grid Partition

Let's consider a typical macromodel with single dielectric containing several conductors. With FDM, the 3-D space within the macromodel is first evenly partitioned. Suppose the segmentation numbers along x, y, z axis are n_x, n_y and n_z, respectively. Fig. 1 shows an example of macromodel with surface partition grids and surface panels. In this subsection, we assume that the grid line is aligned with the surface of inside conductor surface.

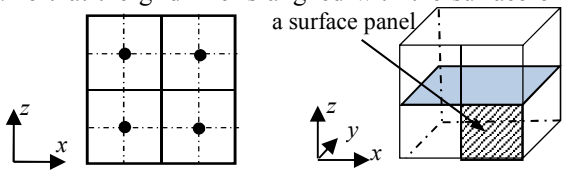

Fig. 1: A macromodel with 2×2×2 finite difference grid. (a) the front face where 4 black dots are surface grid points. (b) the 3-D view.

There are three kinds of grid points: surface grid point, conductor grid point, and other inner grid point. The conductor grid point is that on the surface of conductor, and the point inside conductor is useless for constructing the finite difference equations. Take the grids in Fig. 2 as an example, the 2nd-order differential formula for the normal electric field intensity at surface or conductor grid point is:

$$\frac{\partial U}{\partial x}(x_0) = -\frac{2h_1+h_2}{h_1(h_1+h_2)}u_0 + \frac{h_1+h_2}{h_1h_2}u_1 - \frac{h_1}{(h_1+h_2)h_2}u_2 \quad . \quad (2)$$

For the inner grid point, the 2nd-order derivative of potential is:

$$\frac{\partial^2 U}{\partial x^2}(x_1) = \frac{2}{h_1(h_1+h_2)}u_2 - \frac{2}{h_1h_2}u_1 + \frac{2}{(h_1+h_2)h_2}u_0 \quad . \quad (3)$$

They can be used to represent the electrostatic Laplace equation:

$$\frac{\partial^2 U}{\partial x^2} + \frac{\partial^2 U}{\partial y^2} + \frac{\partial^2 U}{\partial z^2} = 0 \quad , \quad (4)$$

satisfied at each inner point, and the field intensity formula:

$$E_n = -\frac{\partial U}{\partial \vec{n}}, \quad (5)$$

at the surface and conductor grid points.

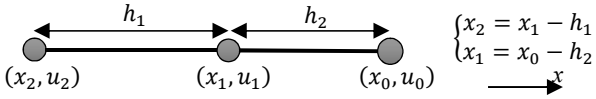

Fig. 2: Illustration of finite difference grid points (the gray balls) and the related distances (h_i) and electrical potentials (u_i). The right most ball is the boundary point or the conductor point.

Therefore, we obtain the FDM equations:

$$\boldsymbol{A}\boldsymbol{U} = \begin{bmatrix} \boldsymbol{A}_{11} & \boldsymbol{A}_{12} & \boldsymbol{A}_{13} \\ \boldsymbol{A}_{21} & \boldsymbol{A}_{22} & \boldsymbol{A}_{23} \\ \boldsymbol{A}_{31} & \boldsymbol{A}_{32} & \boldsymbol{A}_{33} \end{bmatrix} \begin{bmatrix} \boldsymbol{U}_c \\ \boldsymbol{U}_b \\ \boldsymbol{U}_i \end{bmatrix} = \begin{bmatrix} -\boldsymbol{E}_c \\ -\boldsymbol{E}_b \\ \boldsymbol{0} \end{bmatrix} \quad , \quad (6)$$

where $\boldsymbol{U}_c$, $\boldsymbol{U}_b$ and $\boldsymbol{U}_i$ are the voltage of conductor points, boundary points and inner points, respectively. $\boldsymbol{E}_c$ and $\boldsymbol{E}_b$ are the normal electric field intensity of conductor points and boundary points. Because

$$\varepsilon \boldsymbol{S}\begin{bmatrix}\boldsymbol{E}_c\\ \boldsymbol{E}_b\end{bmatrix} = \begin{bmatrix}\boldsymbol{Q}_c\\ \boldsymbol{Q}_b\end{bmatrix} = \boldsymbol{Q} \quad , \tag{7}$$

where $\boldsymbol{S}$ is a diagonal matrix including the areas of surface panels on conductor or macromodel surface, and ε is the dielectric permittivity, we can derive $\boldsymbol{Q} = \widetilde{\boldsymbol{C}}\boldsymbol{U}$. Here,

$$\widetilde{\boldsymbol{C}} = \varepsilon \boldsymbol{S}\begin{bmatrix}\boldsymbol{A}_{13}\boldsymbol{A}_{33}^{-1}\boldsymbol{A}_{31} - \boldsymbol{A}_{11} & \boldsymbol{A}_{13}\boldsymbol{A}_{33}^{-1}\boldsymbol{A}_{32} - \boldsymbol{A}_{12}\\ \boldsymbol{A}_{23}\boldsymbol{A}_{33}^{-1}\boldsymbol{A}_{31} - \boldsymbol{A}_{21} & \boldsymbol{A}_{23}\boldsymbol{A}_{33}^{-1}\boldsymbol{A}_{32} - \boldsymbol{A}_{22}\end{bmatrix} \quad . \tag{8}$$

Because the variables of a same conductor can be condensed to be one quantity, the capacitance matrix $\widetilde{\boldsymbol{C}}$ can be reduced to:

$$\boldsymbol{C} = \boldsymbol{H}_{cond}{}^T \widetilde{\boldsymbol{C}} \boldsymbol{H}_{cond} \quad , \tag{9}$$

where $\boldsymbol{H}_{cond}$ is a cohesion matrix relating panel variables on a conductor to its single variable. The resulting $\boldsymbol{C}$ is the desired macromodel capacitance matrix.

B. Handling Misaligned Conductors

When there is a conductor not aligned to FDM grid, extra partition points are added to designate the position of conductor surface, as shown in Fig. 3. Based on the new nonuniform global grid, the FDM equations are first constructed. Then, the cohesion operation is needed to obtain the desired capacitance matrix corresponding to the original boundary surface division:

$$\boldsymbol{C} = \boldsymbol{H}_{bound}{}^T \boldsymbol{H}_{cond}{}^T \widetilde{\boldsymbol{C}} \boldsymbol{H}_{cond} \boldsymbol{H}_{bound} \quad , \tag{10}$$

where H_{bound} is the cohesion matrix for surface panels.

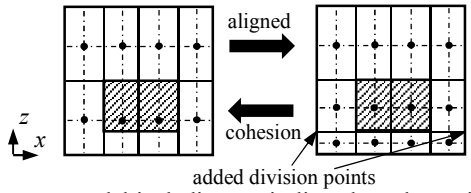

Fig. 3: A macromodel including a misaligned conductor in the front-face view (with a 4×2 partition). Extra division points are added to make the global grid aligned to the conductor surface. And, the cohesion operation is carried out to the macromodel surface panel.

We give the algorithm for generating the macromodel matrix.

Algorithm FDM_CAP

1) Analyze the description file of a macromodel structure. Discretize the macromodel and set up global finite difference grid. If the macromodel is misaligned, insert extra division points to make the conductors aligned.
2) Construct matrix $\boldsymbol{A}$ in (6) by applying (2)~(5) to each grid points.
3) Compute the capacitance matrix $\boldsymbol{C}$ according to (9) or (10).
4) Write capacitance matrix $\boldsymbol{C}$ into database file on hard disk.

III. Implementation and Numerical Results

The FDM_CAP algorithm has been implemented in C++. Either 1st-order or 2nd-order differential formula is used for the electric field intensity at boundary point. As matrix $\boldsymbol{A}_{33}$ is very sparse, the sparse linear solver in [6] is invoked, and OpenMP is utilized for executing parallel computing. For comparison, the BEM in [3] is also tested, which involves Lapack and OpenBLAS to perform fast parallel matrix computation. All experiments are carried out on a Linux server with 2 Intel Xeon 2.4GHz 8-core CPUs. The test cases are as follows.

Case 1: A macromodel containing 4 conductors, one of which is misaligned (see Fig. 4(a)).

Case 2: An empty half-cube macromodel shown in Fig. 4(b).

We first check the sign of matrix entry, and find out that the

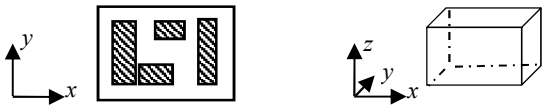

(a) (b)

Fig. 4: Two test macromodel structures. (a) the top view of a structure containing 4 conductors. (b) the 3-D view of an empty half-cube.

results of FDM guarantee that the diagonal entries are positive and off-diagonal entries are negative. In contrast, the results of BEM often violate this property. Then, we check if the sum of each row entries equals to zero. This is not satisfied due to numerical error. In Fig. 5 and 6, the row sums of the macromodel matrices from FDM and BEM are shown. We see that the results from FDM is two orders of magnitude smaller, which means FDM is more compliant with the zero row sum property. While comparing the FDM programs with the 1st-order formula and 2nd-order formula, we see that the latter produces diagonal entries (i.e., total capacitances) closer to those obtained with BEM. Finally, the runtime data in Table 1 validates the efficiency of our FDM solver.

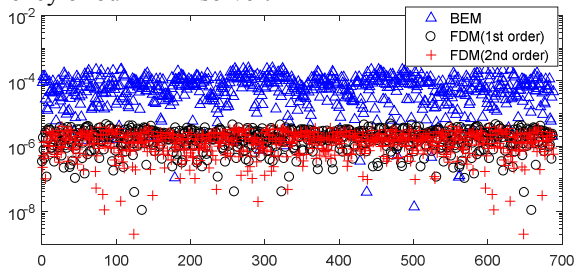

Fig. 5: The absolute value of the sum of matrix entries in the *i*-th row (Case 1). The horizontal axis is the index *i*.

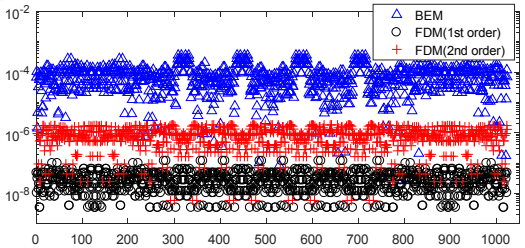

Fig. 6: The absolute value of the sum of matrix entries in the *i*-th row (Case 2). The horizontal axis is the index *i*.

Table 1: Runtime comparison of BEM and FDM based macromodeling.

Test case	#unknown	FDM (s)	#unknown	BEM (s)
Case 1	2036	0.58	932	0.65
Case 2 (coarse)	3072	0.83	1024	1.09
Case 2 (dense)	17100	10.9	3600	12.4

Reference

[1] C. Zhang and W. Yu, "Efficient space management techniques for large-scale interconnect capacitance extraction with floating random walks," *IEEE Trans. Computer-Aided Design*, 32(10): 1633-1637, 2013.

[2] W. Yu, H. Zhuang, C. Zhang, G. Hu, and Z. Liu, "RWCap: A floating random walk solver for 3-D capacitance extraction of VLSI interconnects," *IEEE Trans. Computer-Aided Design*, 32(3): 353-366, 2013.

[3] W. Yu, B. Zhang, C. Zhang, H. Wang, and L. Daniel, "Utilizing macromodels in floating random walk based capacitance extraction," in *Proc. IEEE DATE* , Dresden, Germany, Mar. 2016, pp. 1225-1230.

[4] W. Yu, "RWCap2: Advanced floating random walk solver for the capacitance extraction of VLSI interconnects, " in *Proc. International Conference on ASIC*, Shenzhen, China. Oct. 2013, pp. 162-165.

[5] W. Shi and W. Qiu, "Encrypted profiles for parasitic extraction," US patent No. US8499263B1. Jul. 2013.

[6] T. Davis, *UMFPACK User Guide*. http://www.cise.ufl.edu/research/sparse/umfpack/UMFPACK/Doc/ UserGuide.pdf [Accessed Oct 1, 2016].